11th World Congress on Computational Mechanics (WCCM XI)
5th European Conference on Computational Mechanics (ECCM V)
6th European Conference on Computational Fluid Dynamics (ECFD VI)
E. Oñate, J. Oliver and A. Huerta (Eds)

3D MULTIPHYSICS FEM MODELING OF NANOSECOND PULSED LASER INTERACTION WITH METALLIC FILMS

EVAGGELOS KASELOURIS[1,2], IOANNIS K. NIKOLOS[2], YANNIS ORPHANOS[1,3], EFTHIMIOS BAKAREZOS[1,4], NIKOLAOS VAINOS[3], NEKTARIOS A. PAPADOGIANNIS[1,4], MICHAEL TATARAKIS[1,5] AND VASILIS DIMITRIOU[1,6]

[1]TEI of Crete, Centre for Plasma Physics & Lasers, 73133 Chania, 74100 Rethymno, Greece
v.kaselouris@chania.teicrete.gr, yorphanos@staff.teicrete.gr, bakarezos@staff.teicrete.gr
npapadogiannis@staff.teicrete.gr, m.tatarakis@chania.teicrete.gr, dimvasi@chania.teicrete.gr and
http://www.cppl.teicrete.gr

[2]TUC, School of Production Engineering & Management, University Campus 73100 Chania, Greece,
jnikolo@dpem.tuc.gr and http://www.dpem.tuc.gr

[3]UoP, Department of Materials Science, 26500 Rio, Greece, vainos@upatras.gr and
http://www.matersci.upatras.gr/

[4]TEI of Crete, Department of Music Technology & Acoustics, 74100 Rethymnon, Greece and
www.teicrete.gr/mta

[5]TEI of Crete, Department of Electronics, 73133 Chania, Greece and
https://www.chania.teicrete.gr/academic/electronics-department

[6]TEI of Crete, Department of Natural Resources & Environment, 73133 Chania, Greece and
https://www.chania.teicrete.gr/academic/natural-resources-department

Key Words: *Finite Element Method - FEM, Multiphysics FEM Coupling, Laser-Matter Interactions, Thin Film-Substrate Structures.*

Summary. The 3D dynamic response of thin metallic film-substrate solid structures excited by a nanosecond laser pulse is studied. A coupled thermal-structural, transient model based on the Finite Element Method (FEM) is developed to give a comprehensive spatiotemporal numerical solution in the three dimensional (3D) space. The model is built in a sophisticated way so as to compute the phase changes of matter, with respect to the material properties and the laser irradiation parameters experimentally used. Mathematical and material modeling, are robustly updated by the help of criterions based on the thermal changes of the target. In order to validate the numerical results, a whole-field experimental dynamic interferometric method is used.

1 INTRODUCTION

The dynamic reaction of matter irradiated by a nanosecond laser pulse source depends on its thermo-physical properties, as well as on the laser pulse characteristics. To understand the complex physical phenomenon of this interaction, various analytical and numerical

approximations have been developed[1-10]. However, numerical methods are more suitable in dealing with more complicated problems involving a number of different parameters. The finite element method is versatile due to its flexibility in modeling complex geometries when the domain changes, the desired precision varies over the entire domain, or the solution lacks of smoothness. FEM modeling provides substantial insights into how temperature gradients and residual stresses are developed during the laser-thin film interaction as well as information concerning time-dependent displacements at multiple locations, therefore is appropriate to model complex multiphysics problems.

Studies by the help of FEM have been carried out to investigate the behavior of thin film surfaces under nanosecond laser pulse excitation[6-10]. Xu et al.[7,8] studied the transient temperature and temperature gradient fields in coating-substrate systems as well as the surface normalized vertical displacements at different source-receiver distances and to the epicenter. Their work is focused on the thermoelastic regime. Oliveira and Vilar[9] simulated the laser ablation of titanium carbide with the aid of a two dimensional (2D) finite element model, based on the heat conduction equation and on the Hertz-Knudsen equation of vaporization. Vasantgadkar et al.[6] developed a 2D finite element model capable to predict temperature distribution and ablation depth by taking into account the absorption of laser radiation in plasma. Both of these studies are focused on the pulsed laser ablation phenomenon and the ablation depth (crater's characteristics).

In this study, a coupled thermal-structural, transient model based on the Finite Element Method (FEM) is developed to give a comprehensive spatiotemporal numerical solution in the three dimensional (3D) space. The model is capable to compute the phase changes of matter, with respect to the material properties and the laser irradiation parameters experimentally used. It offers key insights to physical quantities such as displacements, temperatures, velocities, stresses etc. at every spatiotemporal solution time step. To validate the numerical results, a whole-field experimental dynamic interferometric method is used. This diagnostic technique allows the direct monitoring of the spatiotemporal deformation of a macroscopic area on the surface with ultrahigh lateral resolution.

2 PROBLEM DESCRIPTION

2.1 Regimes of laser matter-interaction

The main regimes for high-power pulse laser irradiation of matter are the thermoelastic, melting and ablation/plasma regime. In the thermoelastic regime the thin film surface deforms after the laser excitation without altering its elastic properties. Absorption of the laser pulse results in an increased localized temperature, which in turn causes thermal expansion and generates surface acoustic waves (SAWs)[11,12]. For greater laser intensities the target surface temperature overcomes its melting point and, therefore, the thermal and optical properties of the irradiated material change. When the target surface temperature overcomes its boiling point, ablation occurs. For incident laser intensities, greater than the ablation threshold, a large amount of electrons, ions and excited neutrals exist in the vaporized material and absorb the laser light forming plasma[13].

2.2 Mathematical formulations

In the absence of convective and radiated energy transport, in order to compute the induced temperature distribution T by the absorption of pulsed laser radiation, the heat conduction equation given in Equation 1 is used; x, y and z are the space coordinates while ρ, C_p, k are the mass density, specific heat at constant pressure and the thermal conductivity of the target material, correspondingly. The sublimation and recoil pressure of material, as well as the transport of molten mass are ignored in this model. The source term Q represents the laser energy absorbed by the sample.

$$\rho(T)C_\rho(T)\frac{\partial T(x,y,z,t)}{\partial t}-\nabla[k(T)\nabla T(x,y,z,t)]=Q(x,y,z,t)-L_i \tag{1}$$

When target's temperature is less than its melting point, the incident laser energy onto the surface is conducted into the solid target. For that period of time latent heat L_i is equal to zero. The localized thermal expansion, due to the generated transient temperature elevation field and the transient temperature gradient field, generates a stress field. Consequently, ultrasonic waves are generated and propagate within the volume of the material.

The time-dependent displacements (U) obey Equation 2 where λ and μ are the Lamé constants and a is the thermoelastic expansion coefficient.

$$\rho\frac{\partial^2 U(x,y,z,t)}{\partial t^2}=\mu\nabla^2 U(x,y,z,t)+(\lambda+\mu)\nabla[\nabla U(x,y,z,t)]-\mathrm{a}(3\lambda+2\mu)\nabla T(x,y,z,t) \tag{2}$$

When the temperature exceeds the melting point, phase change occurs and the latent heat of melting L_m, of the material is activated in Equation 1 (i=m). In the ablation regime, L_m is replaced by L_v, to signify the latent heat of vaporization (i=v).

2.3 Source term

The temporal and spatial distribution of the nanosecond laser source may be described by the functions $F(t)$ and $S(r)$ given in Equation 3:

$$F(t)=e^{-4\ln 2(t/t_0)^2}\quad S(x,y)=e^{-(x^2+y^2/r_0^2)} \tag{3}$$

The source term $Q(x, y, z, t)$, representing the laser energy absorbed by the sample, can be expressed as

$$Q(x,y,z,t)=I_s(t)(1-R)F(t)S(x,y)a_b e^{-a_b z} \tag{4}$$

where $I_s(t)$ is the temporal laser irradiance at the sample, R is the optical reflectivity of the sample, and α_b is the optical absorption coefficient ($1/\alpha_b$ is the optical penetration depth). The laser beam temporal profile is assumed to be of the Gaussian type.

2.4 Plasma absorption parameter

For moderate laser fluences, energies delivered per unit area, the nanosecond laser pulse is usually accompanied by the formation of low temperature plasma. The temporal laser irradiance at the target surface is attenuated due to absorption in the plasma that is formed as a

consequence of laser irradiance. An increase in the absorption as a consequence of plasma heating can be characterized by a single parameter, the density of the absorbed radiation energy E_a [14] . The temporal laser irradiance is given by

$$I_s(t) = I_0 e^{-\Lambda(t)} \tag{5}$$

$$\Lambda(t) = b\,h(t) + d\,E_a(t) \tag{6}$$

where I_0 is the incident laser pulse energy per unit area per second and $\Lambda(t)$ is the optical thickness of the ablation plume expressed by Equation 6, where h is the ablation depth and b, d are time independent coefficients.

3 3D FINITE ELEMENT MODEL

The classical thermal conduction equation for finite elements with the heat capacity matrix [C] and the conductivity matrix [K] can be expressed in terms of vectors based on the finite element method

$$[K]\{T\} + [C]\{\frac{\partial T}{\partial t}\} = \{Q\} - L_i \tag{7}$$

where $\{Q\}$ is the heat source vector, $\{T\}$ is the temperature vector and $\{\partial T/\partial t\}$ is the temperature rate vector. For wave propagation, ignoring damping, the governing finite element equation is

$$[M]\{\frac{\partial^2 U}{\partial t^2}\} + [S]\{U\} = \{F\} \tag{8}$$

where [M] is the mass matrix, [S] the stiffness matrix, $\{U\}$ the displacement vector, $\{\partial^2 U/\partial t^2\}$ the acceleration vector and $\{F\}$ the force vector.

A 3D transient coupled-field multiphysics, thermal-structural, analysis is performed. The 3D quarter symmetric finite element model developed (see Figure 1) simulates a homogeneous, elastic, isotropic metal film-substrate system and its transient response when a single laser pulse interacts with the metallic film. Both thermal and structural fields share the same 3D geometry, meshing and elements, boundary and loading conditions. By the help of a direct coupling method, a single pass solution is achieved, involving one analysis that uses the coupled-field 3D element type SOLID5 of the commercial software ANSYS® 14.5[15]. SOLID5 has eight nodes with up to six degrees of freedom per node. The weak field coupling, used in the proposed approximation, is done through the calculation of the appropriate element matrices and load vectors, resulting from the summation of the element matrices and load vectors described in Equations 7 and 8. In order to include the necessary coupling terms, the governing equation results to the form of Equation 9, where the coupled effects are accounted for load terms F-coupled: *Fc* and Q-coupled: *Qc*. This coupling requires at least two iterations in sequence to achieve a coupled response, one for each of the physical phenomena encountered.

$$\begin{bmatrix} [M] & 0 \\ 0 & 0 \end{bmatrix} \begin{Bmatrix} \{\ddot{u}\} \\ \{\ddot{T}\} \end{Bmatrix} + \begin{bmatrix} 0 & 0 \\ 0 & [C] \end{bmatrix} \begin{Bmatrix} \{\dot{u}\} \\ \{\dot{T}\} \end{Bmatrix} + \begin{bmatrix} [S] & 0 \\ 0 & [K] \end{bmatrix} \begin{Bmatrix} \{u\} \\ \{T\} \end{Bmatrix} = \begin{Bmatrix} \{Fc\} \\ \{Qc\} \end{Bmatrix} \tag{9}$$

A fine mesh is required to resolve the temperature distribution in the film and the irradiated region, since the thickness of the film used is of the order of a fraction of a μm and the heat-affected zone is much smaller than the domain of the material. Special treatment is given to the mesh at the circular area of the laser beam spot, at the limits of which the temperature gradients change rapidly, demanding a smooth locally adaptive fine discretization[16]. The dynamic thermal effects, resulting from the heat conduction, are responsible for the structural response of matter around this area. A second larger circular area encloses the irradiated zone and creates the appropriate continuum smooth space, needed for the generation and propagation of SAWs. These assumptions result to a locally adaptive fine mesh of 20160 elements in the quarter circular domain of radius 85μm and a total of 27360 elements in the whole volume of the Au thin film. The whole sample is discretized to a total number of 88920 elements.

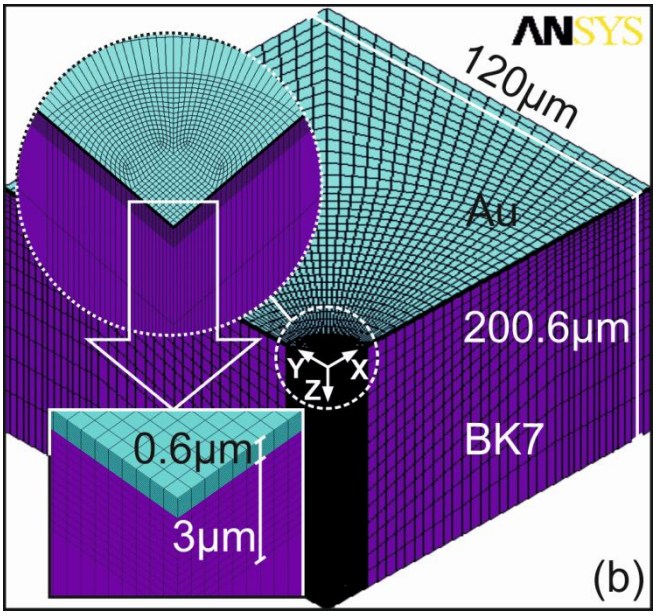

Figure 1: 3D quarter symmetric finite element model details

The initial temperature is assumed to be the ambient temperature. Symmetry displacement loads are applied to the corresponding YZ and XZ planes of symmetry (Figure 1), and heat flux is set to zero because of the quarter symmetry of the 3D model. In relation to the loading conditions a heat generation function, as described in Equation 4, is applied on the film body. With respect to the laser parameters, the FWHM of laser temporal extent, t_0, is 6ns, while the FWHM spatial beam radius on the sample surface, r_0, is 11.5μm as experimentally measured. The time dependent problem is solved sequentially, with an incremental time step of 1ns over a time period of 60ns.

The pre-Processing input data are stored and loaded once at the beginning of the simulation process described in Figure 2. The computational time required for each successive time step of 1ns is approximately 1h. The criterions (flags) used are strictly related to the resulting temperature fields, as shown in the decision rhombus boxes of the flow chart. At the end of a particular step, if the temperature of an element is higher than the melting temperature (T_m),

phase change occurs, which is taken into account by considering the latent heat of melting (L_m) in the model. The ablation is assumed to occur when the temperature of the elements is higher than the boiling temperature. Likewise, in this condition the model takes into account the phase change effect by considering the latent heat of vaporization. If the resulting temperature of an element overpasses the boiling point, a group of elements (GTv) to be vaporized, is created. These elements belong to the material removal subdomain that is achieved by the "killing" of GTv. These elements are deactivated by multiplying their stiffness by a severe reduction factor (~$1x10^{-8}$). For laser fluence higher than the ablation threshold, the optical thickness of the ablation plume, $\Lambda(t)$, is considered and Equation 6 is taken into account by the model[6,9]. The plasma coefficients b and d were evaluated to be 1×10^{6} and 1×10^{-4} respectively, by comparing them with experimental results under various conditions.

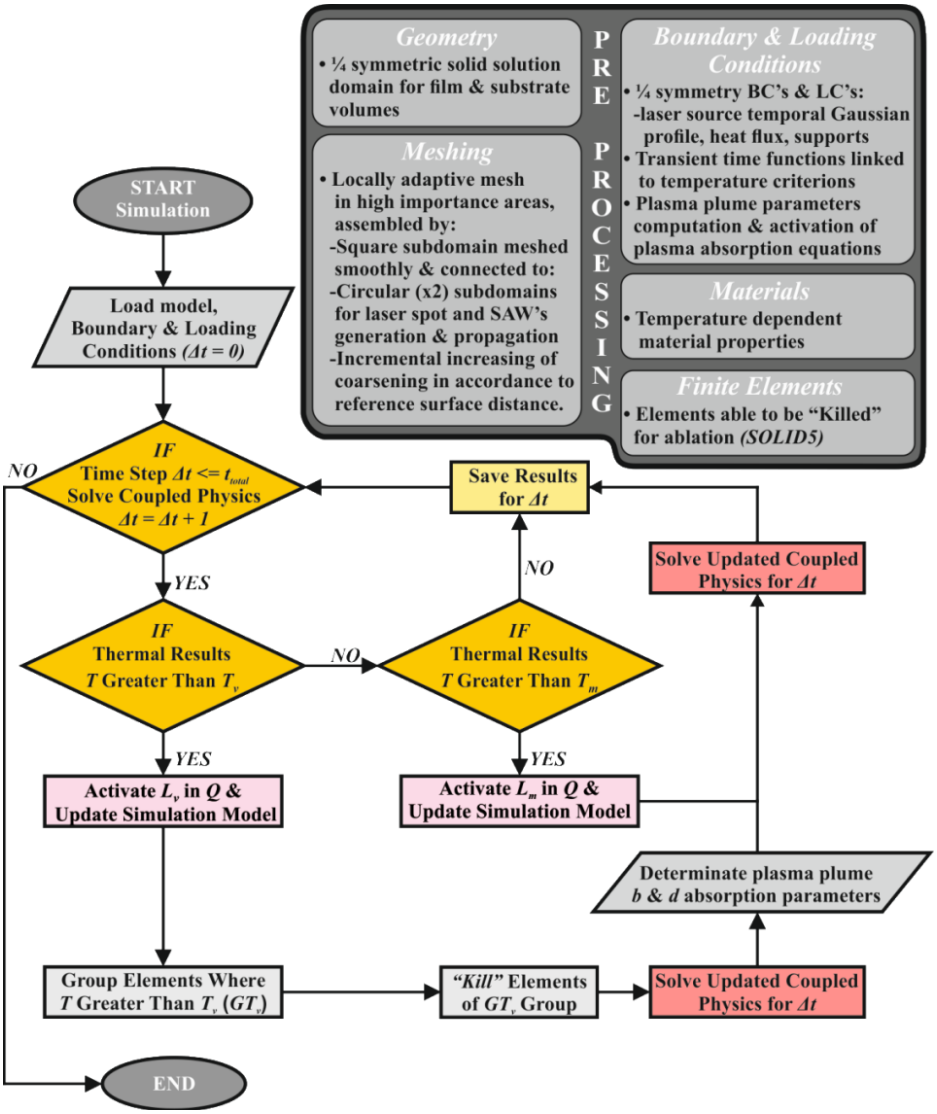

Figure 2: Pre-Processing and Processing Flow chart

4 DYNAMIC IMAGING INTERFEROMETRY

For the experimental investigation of laser generated SAWs, a dynamic imaging interferometric diagnostic technique has been developed and used[17,18]. In Figure 3 the experimental setup is schematically depicted. The pump laser pulses, used for the generation of SAWs, are derived from a frequency-doubled (λ = 532nm) Q-switched Nd:YAG laser, having FWHM time duration of 6ns. The detection pulses are also derived from the aforementioned laser source and are referred to as the probe pulses. The detection scheme incorporates a Michelson interferometer for the interrogation of the sample surface. In addition, a variable optical delay is introduced between the pump and probe pulses. The measurements were performed using a single pulse from the laser system, split accordingly to pump and probe, at room temperature and atmospheric pressure.

The light that reflects off the sample surface is collected by means of lenses and is directed for recording by a CCD camera (2452×2054 pixel sensor with 3.45μm square pixel size). A total sample surface of 500μm × 420μm can be examined. The resulting interferograms are recorded at various optical delays in the presence of the induced SAWs. For the extraction of SAWs amplitude information, a 2D FFT is applied to the interferograms resulting in three distinct peaks, at DC and at $\pm f_0$ (f_0 being the carrier spatial frequency of the fringe pattern). The DC and $-f_0$ components are discarded using a filter and then an inverse 2D FFT is applied. This results in an image where the phase, $\varphi(x,y)$, of every pixel of the interferogram is obtained and wrapped into the range of $-\pi$ to $+\pi$. The phase is then unwrapped and converted to the surface displacement d, with $d = \varphi\lambda/(4\pi)$, where λ is the wavelength of the laser. The whole process is accomplished by the help of in-house developed software. The technique allows for a lateral resolution of ~1μm and of ~1nm in the direction vertical to the sample surface.

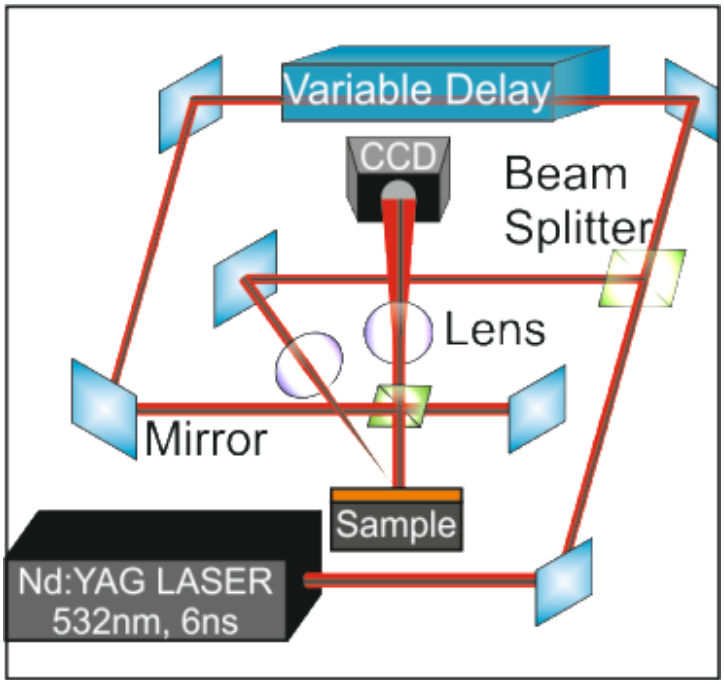

Figure 3: Experimental dynamic imaging interferometry set-up

5 RESULTS

A golden (Au) thin film deposited on BK7 glass substrate was used in this study. The material properties of the sample and the temperature-dependent material properties of gold are given in Table 1. The melting point of Au is 1060^0C, its latent heat of melting L_m is 64kJ/kg, while its latent heat of vaporization L_v is 1600kJ/kg.

Table 1: Material properties of the sample[19,20]

Film-substrate material properties			Temperature dependent properties of Au		
	Au	**BK7 glass**	**Temperature (^{0}C)**	**Thermal conductivity (W/m^{0}C)**	**Specific heat (J/kg^{0}C)**
Density (kg/m^3)	19320	2510	27	317	129
Thermal exp. coef. ($1/^0$C)	$14.2\text{x}10^{-6}$	$7.1\ \text{x}10^{-6}$	127	311	129.5
Young's modulus (GPa)	79	81	227	304	132.3
Poisson's ratio	0.42	0.206	327	298	135.3
			527	284	135.3
			727	270	135.3
			≥927	255	135.3

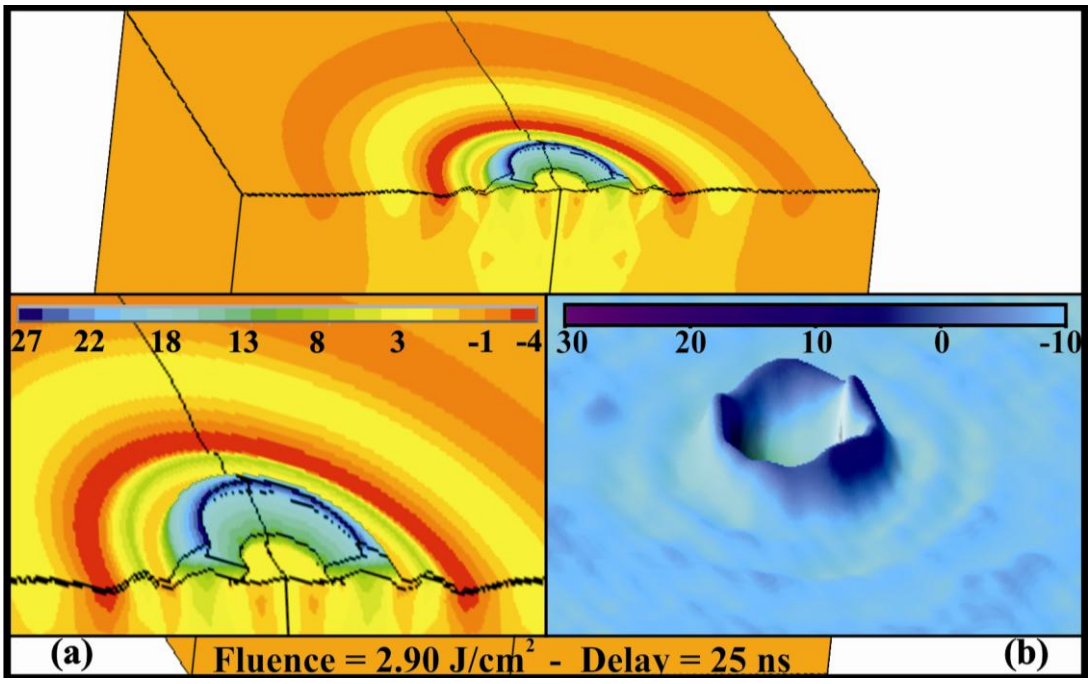

Figure 4: Validation of the model. FEM vs Experimental results

Representative FEM (a) versus Experimental (b) results for laser fluence 2.9J/cm^2 are presented in Figure 4. A crater-type deformation with elevated edges is generated around the laser irradiated region, while SAWs propagate in matter in the form of concentric rings. The

agreement concerning the amplitude of the SAWs and their distance from the epicenter as well as the ablation depth validates the numerical model. The same holds for the elastic and melting regime, indicating that the 3D FEM model is capable to describe the dynamic response of a solid target in the thermoelastic, melting and plasma/ablation regimes, depending upon the laser energy. As it can be noticed from Figure 4(a) (detailed view of the background image) the 3D model offers insights to the whole solid structure, where the transverse propagation of SAWs is observed, while the experiment is capable to monitor the dynamic surface behavior.

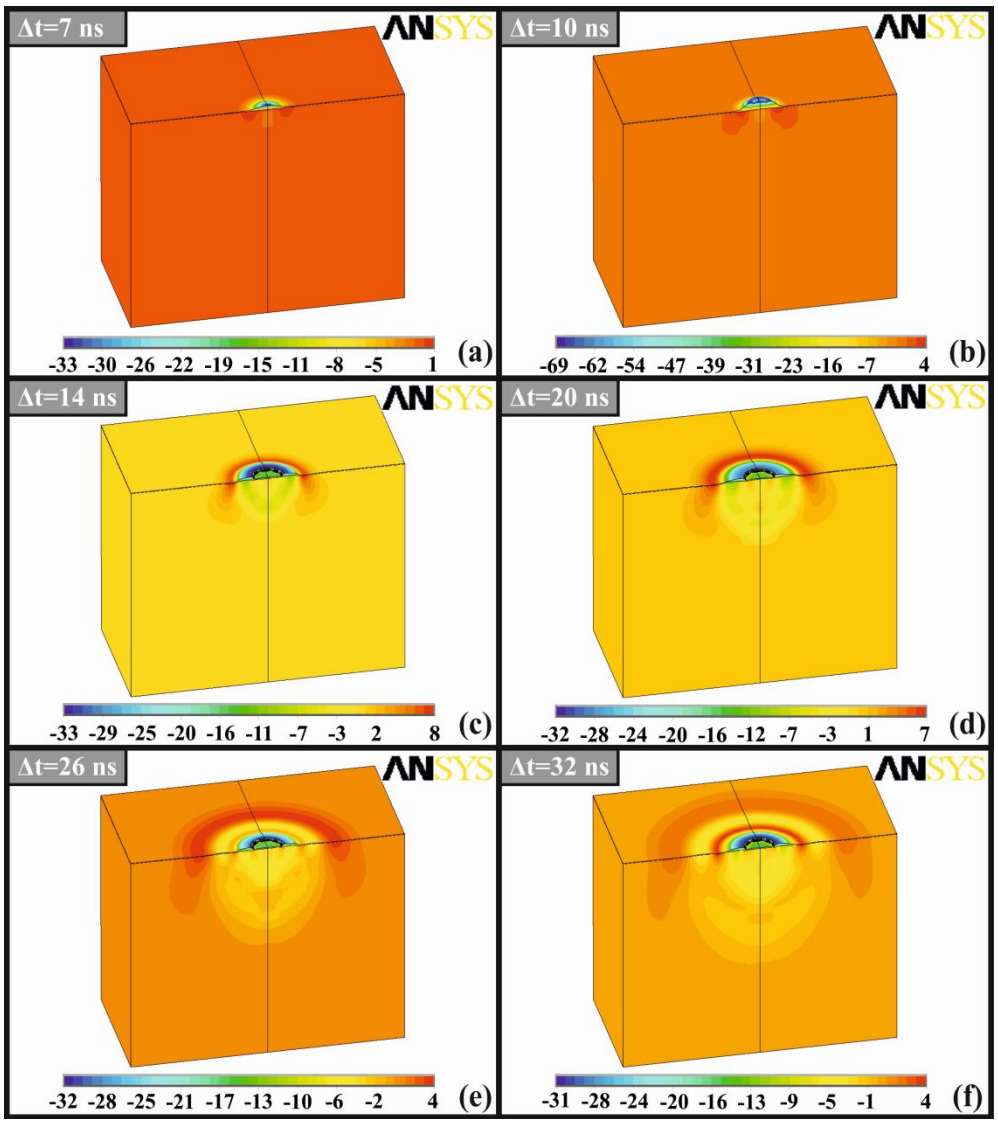

Figure 5: Temporal evolution of solid's deformation (UZ)

In Figure 5 the UZ deformation, in nm, for a half-symmetric model for laser fluence of 3.5J/cm^2 and various *Δt*'s: (a) 7ns, (b) 10ns, (c) 14ns, (d) 20ns, (e) 26ns and (f) 32ns, is presented. For the first 9ns the sample is elastic deformed. In Figure 5(b) the latent heat of

melting is taken into account due to the fact that the temperature overcomes the melting point of the gold. For the Δt = 12ns the latent heat of vaporization is taken into account due to the fact that the temperature overcomes the boiling point of the gold and material is vaporized. In Figure 5(c) the ablated part has been removed and the first SAW is shown. Also in Figure 5(e) a second SAW is created. In Figures 5(d)-(f) the propagation of the SAWs may be observed.

In Figure 6 the vertical surface deformation, obtained by the FEM model simulation for a specific distance 50μm away from the epicenter, is presented as a function of time, for different values of laser fluence. For increasing laser fluence it is observed that the vertical displacement increases, as expected and the peak deformation for both of the SAWs is reached faster in time.

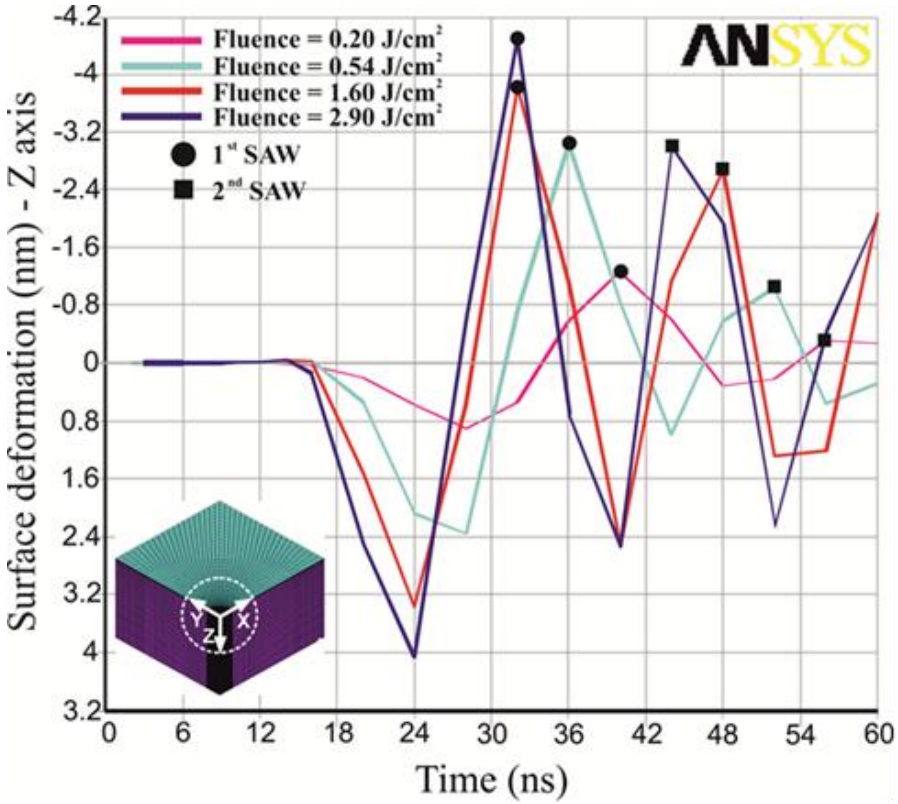

Figure 6: Surface deformation in relation to time

6 CONCLUSIONS

In summary, the 3D spatial and temporal behavior of metallic film-substrate systems excited by a nanosecond laser pulse is investigated in the thermoelastic, melting and ablation regimes utilizing the finite element method. The melting and ablation phenomena are taken into account by a sophisticated 3D FEM model. The thermal conductivity equation is formed so as to include the phase changes of matter related to temperature based criteria. The computational results, validated with experimental data, indicate that the numerical model is capable to fully describe the transient deformation of a solid target and the generation and spatiotemporal evolution of SAWs for all regimes. Furthermore, the model is a valuable tool

for the investigation of the transient mechanical and thermal behavior of any given material. As the used experimental methodology can provide data only at the surface of the observed material, its combination with the proposed FEM model proved to be a valuable addition, as it offers the ability to observe the material behavior in its whole volume.

REFERENCES

[1] Pelivanov, I.M., Kopylova, D.S., Podymova, N.B and Karabutov, A.A. Optoacoustic method for determination of submicron metal coating properties: Theoretical consideration. *J. Appl. Phys.* (2009) **106**:013507-013514.

[2] Singh, R.K. J. Narayan, J. Pulsed-laser evaporation technique for deposition of thin films: Physics and theoretical model, *Phys. Rev. B.* (1990) **41**:8843-8859.

[3] Ho, J.R., Grigoropoulos C.P. and Humphrey J.A. Computational study of heat transfer and gas dynamics in the pulsed laser evaporation of metals. *J. Appl. Phys*. (1995) **78**:4696-4709.

[4] Coulette, R., Lafond E., Nadal, M.H., Gondard, C., Lepoutre, F. and Petillon, O. Laser-generated ultrasound applied to two layered materials characterization: semi-analytical model and experimental validation, *Ultrasonics* (1998) **36**:239-243.

[5] Murray, T.W., Krishnaswamy, S. and Achenbach, J.D. Laser generation of ultrasound in films and coatings, *Appl. Phys. Lett.* (1999) **74**:3561-3563.

[6] Vasantgadkar, N.A., Bhandarkar, U.V. and Joshi, S.S. A finite element model to predict the ablation depth in pulsed laser ablation, *Thin Solid films* (2010) **519**:1421-1430.

[7] Xu, B.Q., Shen, Z.H., Ni, X.W. and Lu, J. Finite element model of laser-generated surface acoustic waves in coating-substrate system, *J. Appl. Phys.* (2004) **95**:2109–2115.

[8] Xu, B.Q., Shen, Z.H., Ni, X.W., Wang, J., Guan, J. and Lu, J. Thermal and mechanical finite element modeling of laser-generated ultrasound in coating–substrate system, *Opt. Laser Technol.* (2006) **38**:138-145.

[9] Oliveira, V. and Vilar, R. Finite element simulation of pulsed laser ablation of titanium carbide. *Appl. Surf. Sci.* (2007) **253**:7810-7814.

[10] Lim, H.S., Yoo, J. FEM based simulation of the pulsed laser ablation process in nanosecond fields, *J. Mech. Sci. Technol.* (2011) **25**:1811-1816.

[11] Scruby, C.E. and Drain, L.E. Laser ultrasonics techniques and applications. Adam Hilger, New York, (1990).

[12] Sorazu, B., Thursby, G., Culshaw, B., Dong, F., Pierce, S.G.,Yang, Y. and Betz, D. Optical generation and detection of ultrasound, *Strain* (2003) **39**:111-114.

[13] Amoruso, S., Bruzzese, R., Spinelli, N. and Velotta, R. Characterization of laser-ablation plasmas, *J. Phys. B: At. Mol. Opt. Phys.* (1999) **32**:R131-R172.

[14] A.V. Bulgakov, N. M. Bulgakova, Thermal model of pulsed laser ablation under the conditions of formation and heating of a radiation-absorbing plasma, *Quantum Electron.* (1999) **29**:433-437.

[15] ANSYS Inc., Coupled-field analysis guide, Release 12.0, Southpointe Canonsburg, April 2009.

[16] Dimitriou, V., Kanarachos, A. and Koulocheris, D. An Approach to Unstructured Finite Element Mesh Generation Using Coons Mapping and Smoothing Techniques, *WSEAS Transactions on Circuits and Systems* (2003) **2**:473-478.

[17] Orphanos, Y., Dimitriou, V. Kaselouris, E., Bakarezos, M., Vainos, N., Tatarakis, M. and Papadogiannis, N. A. An integrated method for material properties characterization based on pulsed laser generated surface acoustic waves, *Microelectron. Eng.* (2013) **112**:249-254.

[18] Dimitriou, V., Kaselouris, E., Orphanos, Y., Bakarezos, M., Vainos, N., Tatarakis, M. and Papadogiannis, N.A. Three dimensional transient behavior of thin films surface under pulsed laser excitation, *Appl. Phys. Lett.* (2013) **103**:114104.

[19] http://www.engineeringtoolbox.com/, last accessed 25 February 2014.

[20] http://www.efunda.com/home.cfm, last accessed 25 February 2014.